Spatiotemporally separating electron and phonon thermal transport in L10 FePt films for heat assisted magnetic recording

D. B. Xu, C. J. Sun, D. L. Brewe, S.-W. Han, P. Ho, J. S. Chen, S. M. Heald, X. Y. Zhang, and G. M. Chow

Articles you may be interested in

Spatiotemporally separating electron and phonon thermal transport in L1$_0$ FePt films for heat assisted magnetic recording

D. B. Xu,[1,2,a)] C. J. Sun,[2,b)] D. L. Brewe,[1] S.-W. Han,[3] P. Ho,[2] J. S. Chen,[2] S. M. Heald,[1] X. Y. Zhang,[1] and G. M. Chow[2,b)]

[1]*Advanced Photon Source, Argonne National Laboratory, Argonne, Illinois 60439, USA*
[2]*Department of Materials Science and Engineering, National University of Singapore, 117576 Singapore, Singapore*
[3]*Department of Physics Education and Institute of Fusion Science, Chonbuk National University, Jeonju 561-756, Republic of Korea*

We report the spatio-temporal separation of electron and phonon thermal transports in nanostructured magnetic L1$_0$ FePt films at the nanometer length scale and the time domain of tens of picosecond, when heated with a pulsed laser. We demonstrate that lattice dynamics measured using the picosecond time-resolved laser pump/X-ray probe method on the FePt (002) and Ag (002) Bragg reflections from different layers provided the information of nanoscale thermal transport between the layers. We also describe how the electron and phonon thermal transports in nanostructured magnetic thin films were separated. © 2014 AIP Publishing LLC. [http://dx.doi.org/10.1063/1.4885428]

I. INTRODUCTION

Nanoscale thermal transport (NTT) at diverse interfaces is a major concern in the design of functional complex nanostructures and nanodevices. It has been known that both electron and phonon contribute to the thermal transport in solid-state materials and across their interfaces. Generally, these two thermal carriers co-exist in the thermal conductance spatially and temporally, the domination of the thermal carriers depends on the nature of the interfaces. Recently, time-resolved lattice dynamics involving one carrier of phonon transport has been investigated in semiconductors[1–5] and multilayer interfaces.[6,7] Electron heat transport was also examined theoretically and experimentally at the metal/metal interface in nanosecond time scale.[8] Furthermore, the transient thermal transport process in a few picoseconds at the interfaces of metal/semiconductor was understood in terms of electron-phonon coupling,[9–11] electron scattering,[12] and phonon scattering,[13] in both electron-phonon equilibrium process and, subsequent, heat transport process across multiple interfaces. The earlier studies demonstrated that NTT in dielectric and metal media were mainly carried by phonon and electron, respectively. However, for NTT involving both electron and phonon, spatiotemporal thermal transports are still unclear. In order to probe and control the dynamic thermal processes in complex nanostructures, a new method for spatiotemporally separating electron and phonon thermal transport is highly desirable from both scientific understanding and nano-engineering applications.[7] Since both phonon and electron NTT result in the lattice distortion, picosecond time-resolved X-ray diffraction can describe the lattice dynamics, which is a very useful route to gain deeper insight into the nature of NTT.[14]

L1$_0$ FePt magnetic thin film is a promising media material for heat assisted magnetic recording (HAMR) due to its high magnetic anisotropy and high corrosion resistance.[15] A laser is used to temporarily heat the media films to reduce its switching field to become lower than the magnetic field of the writing head for data recording, and then the HAMR media need to cool down rapidly to room temperature for data storage. Therefore, a heat-sink layer such as an Ag (002) film is required in HAMR media to achieve the high cooling rate and also have compatible crystallographic texture in order to induce the L1$_0$ FePt (001) epitaxial growth. In this study, the L1$_0$ FePt HAMR media were made with Ag (002) heat-sink layers on MgO (001) substrate, the metal-metal interface was formed by the FePt magnetic layer and the Ag thermal sink layer, whereas the metal-dielectric interface consisted of the Ag layer and the dielectric MgO substrate. We show that the lattice dynamics measured using the picosecond time-resolved laser pump/X-ray probe on the FePt (002) and Ag (002) Bragg reflections provided the information of NTT. Further, we describe how the electron and phonon thermal transports in nanostructured magnetic thin films were separated at the time domain of tens of picosecond and length scale of nanometer.[16]

II. EXPERIMENT

For consistency, a series of nanostructured thin films with structure of Ta (2 nm)/FePt (30 nm)/Ag (80 nm), Ta (2 nm)/FePt (30 nm), and Ta (2 nm)/Ag (80 nm) films was grown on (001) MgO single crystal substrates (1 cm × 1 cm × 0.5 mm) using magnetron sputtering at elevated temperatures.[17] The deposition temperature and pressure for Ag, FePt, Ta were 250 °C, 400 °C, room temperature and 1.5 mTorr, 10 mTorr, 10 mTorr, respectively. The top 2 nm Ta layer acts as a capping layer to minimize oxidization. The X-ray diffraction (XRD) θ–2θ scans in Fig. 1 show that Ag with (001) texture along the film normal was successfully

a)Author's current address: Seagate Singapore. Electronic address: dongbin.xu@seagate.com.
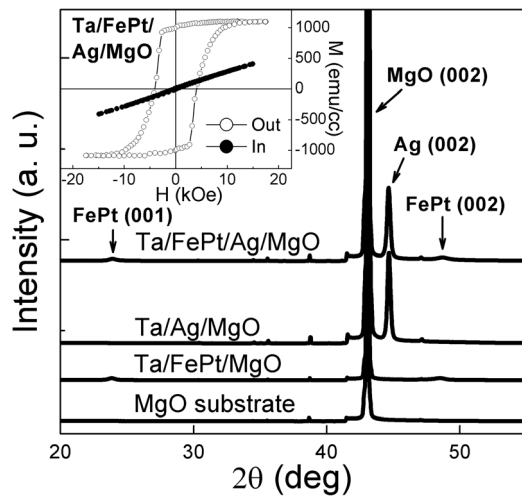b)Authors to whom correspondence should be addressed. Electronic addresses: cjsun@aps.anl.gov and msecgm@nus.edu.sg.

FIG. 1. θ-2θ XRD scans for Ta/FePt/Ag/MgO, Ta/Ag/MgO, Ta/FePt/MgO, and MgO substrate. The inset shows the out-of-plane and in-plane hysteresis loops for Ta/FePt/Ag/MgO measured with VSM at room temperature. M and H represent magnetization in emu/cc and magnetizing field in kOe, respectively.
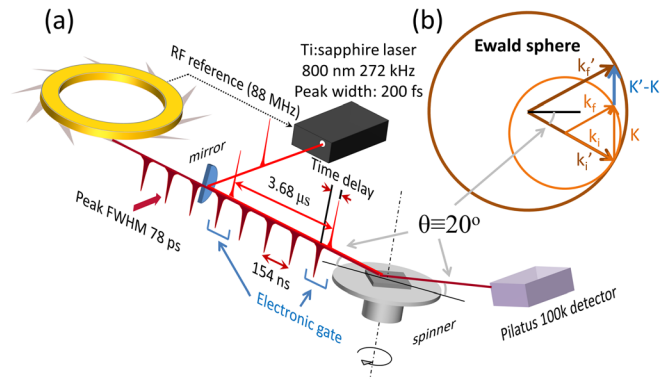

FIG. 2. The setup of TR-XRD measurements. (a) An illustration of the setup for TR-XRD measurement in real space. Timing changes are made by shifting phase of radio frequency reference used in laser feedback loop. (b) A schematic diagram for TR-XRD measurement in reciprocal space, here, θ was fixed at 20° and photon energy of X-ray was varied for measurement. Where $\boldsymbol{K}$ ($\boldsymbol{K'}$) is a reciprocal lattice vector, $\boldsymbol{k_i}$ ($\boldsymbol{k_i'}$) and $\boldsymbol{k_f}$ ($\boldsymbol{k_f'}$) are the wave vectors of the incident and the diffracted beams at photon energy of E (E'), respectively. They fulfill the relations $\boldsymbol{K} = \boldsymbol{k_f} - \boldsymbol{k_i}$, $\boldsymbol{K'} = \boldsymbol{k_f'} - \boldsymbol{k_i'}$ and E < E'. The diffraction occurs only when reciprocal lattice vector $\boldsymbol{G} = \boldsymbol{K'} - \boldsymbol{K}$. Here, the time spacing between pulses is only for illustration, the time scales for laser and X-ray pulses are different.

deposited on the MgO substrates. The existence of superlattice peaks (001) of FePt in Ta/FePt/Ag/MgO and Ta/FePt/MgO samples suggested that the $L1_0$ ordered FePt with (001) texture was achieved on both Ag (002) and MgO (002). The X-ray rocking curves of Ag (002) and FePt (002) had the full width at half maximum (FWHM) of 0.252° and 1.434°, respectively. This implied a very good texture in (001) direction for both Ag and FePt layers, which is preferred in the perpendicular magnetic recording for HAMR. Consistently, the in-plane and out-of-plane vibrating sample magnetometer (VSM) hysteresis loops at room temperature (see inset of Fig. 1) revealed high perpendicular anisotropy of the $L1_0$ FePt layer. Here, the in-plane hysteresis loop was not saturated due to the extremely high anisotropy field of $L1_0$ FePt, which is typically around $70 \sim 80$ kOe.

In order to temporally investigate the electron and phonon mediated thermal transport in sub-nanosecond time scale and determine the individual thermal carrier dominance and contribution in hybridized interfaces, picosecond time-resolved laser pump/X-ray probe diffraction was performed at sector 20-ID-C of the Advanced Photon Source (APS) as shown in Fig. 2. The specular X-ray diffraction was performed by fixing the angles of incident and reflected X-rays, and changing the X-ray energy; a schematic diagram in reciprocal space for our measurement is shown in Fig. 2(b). The X-ray energy was selected using a Si (111) monochromator with an energy resolution of about 1.5 eV. Specifically, a local area on the sample surface illuminated by the laser pulse with an elliptical spot ($\sim 120 \mu m$ in major axis and ~ 80 in minor axis) was probed by an X-ray beam (5 μm) with $\theta = 20°$ as shown in Fig. 2(a). The pulsed laser with a width of 200 femtosecond (fs) and the laser power of 300 mW was derived from the output of Ti-sapphire laser system at a repetition rate of 272 kHz that matched the single bunch repetition rate of the APS storage ring. The laser pulse was synchronized with a particular X-ray pulse and a Pilatus area detector was gated to collect the diffraction data from

this pulse. The X-ray beam from the synchrotron was focused to 5 μm diameter with a Kirkpatrick-Baez mirror system. During the measurement, the samples were spun with a spinner to avoid multishot degradation. By using this configuration, the relative directions of X-ray, laser, and sample were fixed.

III. RESULTS AND DISCUSSION

The contour plots of the FePt (002) diffraction peak for Ta/FePt/MgO and Ta/FePt/Ag/MgO as a function of the time delay between X-ray and laser pulses from −264 ps to 1038 ps are shown in Figs. 3(a) and 3(c). Figs. 3(b) and 3(d) show the diffraction curves at three marked time delays with corresponding colors, highlighting the Bragg peak's shift in energy when the laser was applied. The diffraction peaks were fitted with Gaussian curves to describe the normal symmetric distribution. Using this fitting as shown in solid lines in Figs. 3(b) and 3(d), the quantitative information about the diffraction energy position and peak integrated intensity may be derived. The lattice expansions in c direction derived from the energy shifts in Figs. 3(a) and 3(c) are shown in Fig. 3(e).

When the film surface was exposed to an ultra-short laser pulse, the laser pulse initially interacted with the electrons in FePt generating hot carriers in the film by transferring the photon energy to the kinetic energy of electrons. This process was typically finished within a few 100 fs. After about $0.1 \sim 1$ ps, most of the energy was transferred from the hot electrons to the lattice (phonons) and equilibrium was reached between them.[9,10] Several studies showed that the hot electron diffusion before transferring the energy to lattice cannot be ignored.[18,19] These studies showed for an Au film, the heat could be transferred with electron diffusion at a velocity close to the Fermi velocity of electrons,[18] and for an Al film electrons could reach a depth of around 70 nm
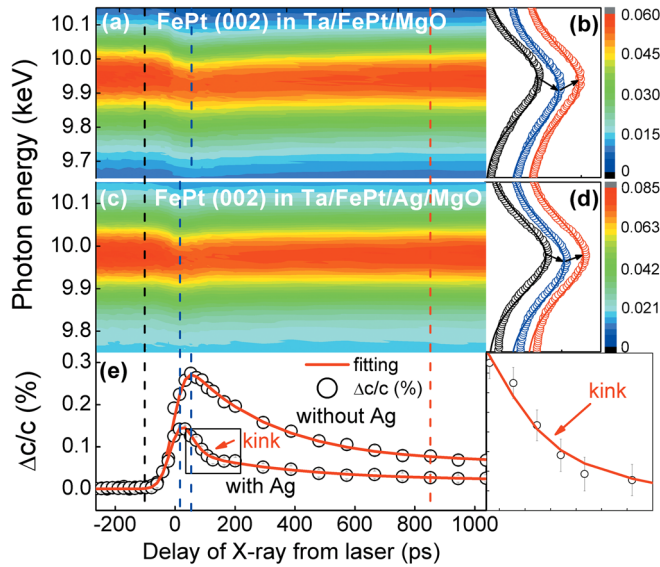
FIG. 3. Lattice dynamic as a function of X-ray delay from laser for FePt (002) in Ta/FePt/MgO and Ta/FePt/Ag/MgO. The contour plots are the FePt (002) diffractions in (a) Ta/FePt/MgO and (c) Ta/FePt/Ag/MgO as a function of X-ray delay from laser. (b) and (d) XRD curves together with the Gaussian fittings at three time delays as marked in dashed lines with corresponding colors. (e) The lattice expansion of FePt (002) in Ta/FePt/MgO and Ta/FePt/Ag/MgO as a function of X-ray delay from laser and its corresponding fitting lines as described in the text. Here, error bars were derived from Gaussian fitting.

before transferring energy to the lattice.[19] In our experiment, the penetration depth of the 800 nm laser in FePt was ~15 nm and hence the heat energy was easily transferred through the entire FePt film within a few ps via electron diffusion. Considering the minimum time step size (~18 ps) in our measurement, instantaneous heating of the whole FePt film was achieved once the laser pulse was applied. The subsequent thermal decay process was treated as the heat diffusion from the entire thermally equilibrated top layer into the underlayer/substrate.

Here, we interpret the thermal decay process based on a two-layer model, where heat diffused from the upper layer into the lower layer through a thermal resistance by assuming a uniformly heated upper layer. This model is suitable to our case since the whole FePt layer (upper layer here) was uniformly heated in the first few ps as discussed and the subsequent thermal decay process was mainly dominated by heat diffusion. In order to quantitatively interpret the nanoscale thermal transport in the interface, a decay function was derived from a heat diffusion equation[20] $\frac{\partial^2 T_s}{\partial z^2} = \frac{1}{\alpha_s} \frac{\partial T_s}{\partial t}$ (here, T is the temperature, α_s is the thermal diffusivity, and $\alpha_s = \frac{k_s}{\rho_s c_s}$, where k represents the thermal conductivity, ρ the mass density, c the heat capacity, subscript s denotes the lower layer (underlayer or substrate). Two boundary conditions including (i) the conservation of heat flux condition at interface and (ii) the thermal resistance condition at interface were considered in the process of derivation. By using the Laplace transform at the limit, where interface resistance was dominant[20] and assuming a constant thermal expansion coefficient ($\Delta T \propto \frac{\Delta c}{c}$), the equation was derived as

$$\left(\frac{\Delta c}{c}\right)_t = \left(\frac{\Delta c}{c}\right)_{t=0} \times \exp\left[-t \times \left(\frac{\rho_f e_f d_f}{G_{th}}\right)^{-1}\right], \quad (1)$$

where $\left(\frac{\Delta c}{c}\right)_{t=0}$ is lattice expansion at $t=0$ ps, while $\left(\frac{\Delta c}{c}\right)_t$ is the lattice expansion at t (the time delay of X-ray from laser in ps), here, the denominator a is the corresponding lattice parameter before expansion. τ_i is the exponential time-constant in ps and $\tau_i = \frac{\rho_f e_f d_f}{G_{th}}$, here, d is the thickness, and the subscript f denotes the upper layer in the two-layer model. The exponential decay equation used in the study of Plech *et al.*[21] showed a good capability to calculate the interface heat transfer coefficient for Ag nanoparticles embedded in an Au matrix, these works were performed on nanoparticles with mean diameters from 20 to 100 nm using 100 ps X-ray pulses from a synchrotron, both the spacio and temporal dimensions in that study[21] are comparable with the current study.

Generally, the decay function may be described as $f(t) = \sum_i \left(\frac{\Delta c_i}{c}\right)_{t=0} \times \exp(-\frac{t}{\tau_i})$ for the independent decay paths ($A \to B, C...$). By further convolution of the exponential decay function (Eq. (1)) with the Gaussian-like X-ray temporal profile $G(t) = \frac{1}{\sqrt{2\pi}\sigma}\exp(-\frac{t^2}{2\sigma^2})$, where $\sigma = \frac{1}{2\sqrt{2\ln 2}}$ $\cdot FWHM$, $\sigma = 33.1$ ps for the 24-bunch operation mode of the APS, the final fitting equation may be derived for parallel decay paths by summing all paths

$$\left(\frac{\Delta c}{c}\right)_{data} = \sum_{i=1,2,3} \left\{\frac{1}{2} \times \left(\frac{\Delta c_i}{c}\right)_{t=0} \times \exp\left(\frac{\sigma^2}{2\tau_i^2} - \frac{t}{\tau_i}\right)\right.$$
$$\left. \times \left[erf\left(\frac{t}{\sqrt{2}\sigma} - \frac{\sigma}{\sqrt{2}\tau_i}\right) + 1\right]\right\}, \quad (2)$$

where $\left(\frac{\Delta c}{c}\right)_{data}$ is the lattice expansion measured in the experiment broadened by the X-ray temporal profile, $\left(\frac{\Delta c_i}{c}\right)_{t=0}$ is the lattice expansion after deconvolution at $t=0$ ps. The thermal conductance G_{th} for the interface may be derived from $G_{th} = \frac{\rho_f e_f d_f}{\tau_i}$, where τ_i is the exponential time-constant in ps. $erf(x)$ is the error function. The choice of detecting X-ray diffraction signal eliminated the use of laser frequency parameter for calculation as in the precious study,[22] where laser was used for both pump and probe signals. The elimination of laser frequency parameter rendered further analyses and fitting easier. The decay curves for FePt (002) in Ta/FePt/MgO and Ag (002) in Ta/Ag/MgO and Ta/FePt/Ag/MgO were also fitted with Eq. (2) for comparison.

The fitting plots are shown in Fig. 3(e) as red curves. A constant background was also included in the fitting by assuming constant temperature (infinite thermal conductivity) of MgO substrate. Except for this, one relaxation time was needed for fitting of FePt (002) in Ta/FePt/MgO. While for FePt (002) in Ta/FePt/Ag/MgO, an obvious kink, implying a two-step relaxation, can be seen from Fig. 3(e). By choosing two relaxation times, a good fit was achieved within the error bars of the experimental data points. The thermal conductance was, then, calculated and is shown in Table I using the typical values (FePt: $\rho = 15$ g/cc, $c = 50$ J·mol^{-1}·K^{-1}, $d = 30$ nm; Ag: $\rho = 10.5$ g/cc, $c = 25.4$ J·mol^{-1}·K^{-1}, $d = 80$ nm).

TABLE I. Exponential time-constants as well as corresponding thermal conductances for single or multiple interfaces thermal transport in different layer structures from the fittings. Standard error bars were derived during fitting with Eq. (2).

Layer structure	Lattice plane	Interface	Exponential time-constant (ps)	Thermal conductance (W·m^{-2}·K^{-1})
Ta/FePt/Ag/MgO	FePt (002)	FePt/Ag	24 ± 7	$3.8 \pm 1.2 \times 10^9$
		Ag/MgO	367 ± 115	$5.4 \pm 1.9 \times 10^8$
Ta/FePt/MgO	FePt (002)	FePt/MgO	290 ± 27	$3.1 \pm 0.3 \times 10^8$

The origin of these two relaxation times in Ta/FePt/Ag/MgO is discussed as follows. It is expected that the thermal conductance at a metal/metal interface would be high because both sides had many free electrons that could transfer their thermal energy at a velocity close to Fermi velocity, where no significant change of density of states with temperature was assumed.[18] This was electron-dominated thermal transport as shown in Figs. 4(a) and 4(b) as red line. Another resistance for electron thermal transport was electron-phonon coupling in sink layer (Ag) that contributed to the electron thermal resistance.[23] In order to consider both contributions, the thermal resistance to the electron-dominated thermal transport included both contributions from interface to electron-phonon coupling in Ag. The contribution of phonons to thermal transport in metal was typically below 10%, although there is still no agreement on a precise value.[24,25] The situation becomes complicated when considering the thermal transport through a metal/dielectric interface such as Ag/MgO or FePt/MgO interface since phonons may play a more important role. In this case, we proposed two mechanisms to describe the thermal transport: (i) electrons and phonons were coupled at the metal-nonmetal interface;[26–28] (ii) electrons and phonons exchanged the thermal energy in the metal film first, then transferred the energy from metal to dielectric material via phonon-phonon interaction.[29] Both processes shown in Fig. 4(b) as blue lines were considered as phonon-dominated thermal transport. Electron-dominated and phonon-dominated thermal transports at the FePt/Ag and Ag/MgO interfaces yielded the two relaxation processes in our measurement as shown in Fig. 4(a). It also strengthened our argument that the electron-dominated thermal transport occurred first, which was then followed by the phonon-dominated thermal transport. For comparison, the thermal conductance for a Al/Cu interface is $\sim 3 \times 10^9$ W·m^{-2}·K^{-1}, while that for Cu/Al$_2$O$_3$ is $\sim 2 \times 10^8$ W·m^{-2}·K^{-1} at room temperature.[8] This is consistent with our results for FePt/Ag and Ag/MgO interfaces, respectively. The small increase in G_{th} compared with previous reported values for Al/Cu and Cu/Al$_2$O$_3$ interfaces was probably due to the relatively high temperatures reached in the measurements. The increase of thermal conductance with temperature had also been reported.[8] By using the typical bulk thermal expansion coefficient (Fe: 11.8×10^{-6} K^{-1}, Pt: 8.8×10^{-6} K^{-1}, FePt (averaged from elemental crystal of Fe and Pt): 10.3×10^{-6} K^{-1}), the maximum temperature of FePt in Ta/FePt/MgO was roughly estimated to be approximately 882 K from the
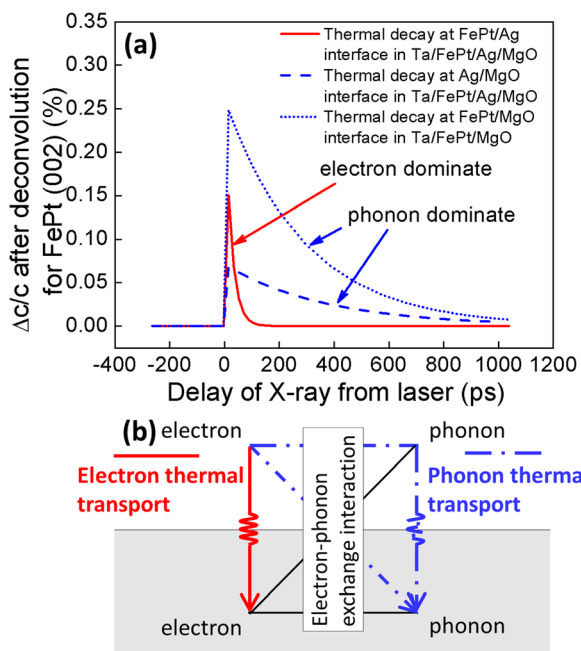

FIG. 4. Separated electron and phonon thermal transport in terms of deconvoluted exponential decays. (a) Deconvoluted exponential decay curves plotted with the parameters derived from the fitting curves in Fig. 3(e). (b) A schematic diagram for electron and phonon thermal transport at interface. The electron-phonon interactions in the same layer and at the interface are treated as electron-phonon exchange interaction.
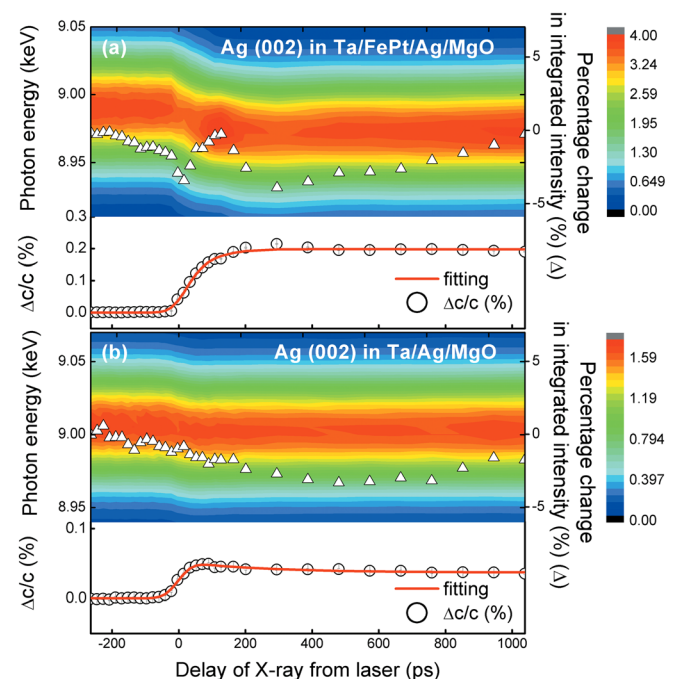

FIG. 5. Lattice dynamic as a function of X-ray delay from laser for Ag (002) in Ta/FePt/Ag/MgO and Ta/Ag/MgO. Contour plots, percentage change in integrated intensity (Δ), and variations of lattice expansion with fitting lines for Ag (002) in (a) Ta/FePt/Ag/MgO and (b) Ta/Ag/MgO as a function of X-ray delay from laser. Here, error bars were derived from Gaussian fitting.

equation $T = 300K + \frac{1+\nu}{1-\nu} \times \frac{\Delta c}{c} \times \frac{1}{\alpha}$ by assuming a temperature-independent α. Here, ν is passion ratio and a typical value of 0.33 was used for FePt.[30] When using the Ag heat sink layer, the maximum temperature estimated was around 600 K. The deconvoluted data for two relaxation processes during thermal decay of FePt (002) for Ta/FePt/Ag/MgO together with that of FePt (002) for Ta/FePt/MgO are shown in Fig. 4(a).

Further investigation on lattice expansion and variation of integrated intensity of Ag (002) with X-ray delay from laser illustrated in Fig. 5 was consistent with the previous discussion. Compared with the Ag layer without FePt on top, the Ag in Ta/FePt/Ag/MgO had a larger expansion due to the heat transported from FePt layer. The integrated intensity reached its maximum at around 100 ps delay, which corresponded to the time point, where heat flow from FePt vanished as shown in Fig. 3. Beyond 100 ps, the heat dissipation would only be dominated by phonon thermal transport at the Ag/MgO interface. This was because that FePt and Ag layers had reached equilibrium temperature through electron dominated thermal transport, the subsequent thermal transport was dominated by the temperature gradient at Ag/MgO interface through the relative slower phonon-dominated thermal transport.

IV. CONCLUSION

A good understanding of thermal transport especially at the interface in the nanometer scale remains highly desirable.[31] Our study showed the viability of separating the electron and phonon contributions to the thermal transport in various interfaces of FePt-Ag films during a single measurement. The electron and phonon thermal transports were separately investigated. It is suggested that a model incorporates ballistic phonons and electrons and their stochastic nature should be further developed for a more realistic description at these spacio-temporal scales.

[1] C. Rose-Petruck, R. Jimenez, T. Guo, A. Cavalleri, C. W. Siders, F. Rksi, J. F. Squier, B. C. Walker, K. R. Wilson, and C. P. J. Barty, Nature **398**, 310 (1999).

[2] A. Cavalleri, C. W. Siders, F. L. H. Brown, D. M. Leitner, D. M. Tóth, J. A. Squier, C. P. J. Barty, K. R. Wilson, K. Sokolowski-Tinten, M. H. Hoegen, D. V. D. Linde, and M. Kammler, Phys. Rev. Lett. **85**, 586 (2000).

[3] A. M. Lindenberg, I. Kang, S. L. Johnson, T. Missalla, P. A. Heimann, Z. Chang, J. Larsson, P. H. Bucksbaum, H. C. Kapteyn, H. A. Padmore, R. W. Lee, J. S. Wark, and R. W. Falcone, Phys. Rev. Lett. **84**, 111 (2000).

[4] D. A. Reis, M. F. DeCamp, P. H. Bucksbaum, R. Clarke, E. Dufresne, M. Hertlein, R. Merlin, R. Falcone, H. Kapteyn, M. M. Murnane, J. Larsson, T. Missalla, and J. S. Wark, Phys. Rev. Lett. **86**, 3072 (2001).

[5] M. Highland, B. C. Gundrum, Y. K. Koh, R. S. Averback, D. G. Cahill, V. C. Elarde, J. J. Coleman, D. A. Walko, and E. C. Landahl, Phys. Rev. B **76**, 075337 (2007).

[6] M. Bargheer, N. Zhavoronkov, Y. Gritsai, J. C. Woo, D. S. Kim, M. Woerner, and T. Elsaesser, Science **306**, 1771 (2004).

[7] Z. Li, S. Tan, E. Bozorg-Grayeli, T. Kodama, M. Asheghi, G. Delgado, M. Panzer, A. Pokrovsky, D. Wack, and K. E. Goodson, Nano Lett. **12**, 3121 (2012).

[8] B. C. Gundrum, D. G. Cahill, and R. S. Averback, Phys. Rev. B **72**, 245426 (2005).

[9] J. K. Chen, W. P. Latham, and J. E. Beraun, J. Laser Appl. **17**, 63 (2005).

[10] L. Guo, S. L. Hodson, T. S. Fisher, and X. F. Xu, J. Heat Transfer **134**, 042402 (2012).

[11] D. A. Luh, T. Miller, J. J. Paggel, and T. C. Chiang, Phys. Rev. Lett. **88**, 256802 (2002).

[12] P. E. Hopkins, J. L. Kassebaum, and P. M. Norris, J. Appl. Phys. **105**, 023710 (2009).

[13] H. Zhao and J. B. Freund, J. Appl. Phys. **105**, 013515 (2009).

[14] D. G. Cahill, P. V. Braun, G. Chen, D. R. Clarke, S. Fan, K. E. Goodson, P. Keblinski, W. P. King, G. D. Mahan, A. Majumdar, H. J. Maris, S. R. Phillpot, E. Pop, and L. Shi, Appl. Phys. Rev. **1**, 011305 (2014).

[15] M. H. Kryder, E. C. Gage, T. W. McDaniel, W. A. Challener, R. E. Rottmayer, G. Ju, Y. T. Hsia, and M. F. Erden, Proc. IEEE **96**, 1810 (2008).

[16] C. J. Sun, D. B. Xu, D. L. Brewe, J. S. Chen, S. M. Heald, and G. M. Chow, IEEE Trans. Magn. **49**, 2510 (2013).

[17] J. S. Chen, J. F. Hu, B. C. Lim, W. L. Phyoe, B. Liu, and G. Ju, J. Appl. Phys. **105**, 07B724 (2009).

[18] S. D. Brorson, J. G. Fujimoto, and E. P. Ippen, Phys. Rev. Lett. **59**, 1962 (1987).

[19] G. Tas and H. J. Maris, Phys. Rev. B **49**, 15046 (1994).

[20] S. Volz, *Topics in Applied Physics: Microscale and Nanoscale Heat Transfer* (Springer, New York, 2007).

[21] A. Plech, S. Kürbitz, K.-J. Berg, H. Graener, G. Berg, S. Grésillon, M. Kaempfe, J. Feldmann, M. Wulff, and G. V. Plessen, Europhys. Lett. **61**, 762 (2003).

[22] D. G. Cahill, Rev. Sci. Instrum. **75**, 5119 (2004).

[23] W. Wang and D. G. Cahill, Phys. Rev. Lett. **109**, 175503 (2012).

[24] J. V. Goicochea and B. Michel, in *Proceedings of the 27th Annual IEEE Semiconductor Thermal Measurement and Management Symposium (SEMI-THERM), San Jose, CA, USA, 2011*, pp. 155–160.

[25] B. Feng, Z. Li, and X. Zhang, J. Appl. Phys. **105**, 104315 (2009).

[26] M. L. Huberman and A. W. Overhauser, Phys. Rev. B **50**, 2865 (1994).

[27] A. V. Sergeev, Phys. Rev. B **58**, R10199 (1998).

[28] G. D. Mahan, Phys. Rev. B **79**, 075408 (2009).

[29] A. Majumdar and P. Reddy, Appl. Phys. Lett. **84**, 4768 (2004).

[30] P. V. Lukashev, N. Horrell, and R. F. Sabirianov, J. Appl. Phys. **111**, 07A318 (2012).

[31] D. G. Cahill, W. K. Ford, K. E. Goodson, G. D. Mahan, A. Majumdar, H. J. Maris, R. Merlin, and S. R. Phillpot, J. Appl. Phys. **93**, 793 (2003).